Modeling Xylene Reactions over ZSM-5 Zeolite in a Riser Simulator: 1,3 versus 1,2-Methyl Shift

S. Al-Khattaf*, N. M. Tukur and A. Al-Amer

Department of Chemical Engineering
King Fahd University of Petroleum & Minerals
Dhahran 31261, Saudi Arabia.

Abstract

Xylene transformation reactions have been investigated over ZSM-5 zeolite in a riser simulator that mimics closely the operation of commercial fluidized-bed reactors. Two reaction schemes have been used to model the transformation reactions. The first based on triangular reaction path which assumes a direct interconversion between *o*- and *p*-xylene isomers (1,3-methyl shift), and a second scheme that assumes the reactions to proceed via 1,2-methyl shift only (*o*-xylene *m*-xylene *p*-xylene). The rate constants and activation energies are obtained from simplified kinetic models based on the isomerization of the pure xylene isomers using the "Time on Stream" decay model. The results provide ample evidence to suggest that direct interconversion between *o*- and *p*-xylene isomers (a 1,3-methyl shift) occurs with the same rate as the conversion of *m*- to *o*-xylene (a 1,2-methyl shift) over ZSM-5 zeolite catalyst, and the 1,3-methyl shift reaction path is a better representation of the xylene isomerization mechanism in ZSM-5 zeolite than the 1,2-methyl shifts only. In addition, the riser simulator and the modeling procedures employed have shown to be very effective in investigating xylene isomerization kinetics.

Keywords: Xylene transformation, Kinetic modeling, fluidized-bed reactor, ZSM-5, isomerization, disproportionation

*Corresponding author. Tel.: +966-3-860-1429; Fax: +966-3- 860-4234
E-mail address: skhattaf@kfupm.edu.sa

1. Introduction

The demand for *p*-xylene as a starting raw material for the manufacture of terephthalic acid (PTA) and dimethyl terephthalate (DMT) has increased tremendously over the past years. Nearly all *p*-xylene recovered from petroleum in the US is consumed in the manufacture of PTA and DMT, which are used to manufacture polyethylene terephthalate (PET). Other miscellaneous uses include solvent use, manufacture of di-paraxylene and herbicides. Total U.S. consumption of *p*-xylene is projected to grow at 3.5 percent annually through 2004. With no apparent capacity additions, domestic demand for *p*-xylene will exceed capacity in the near future. [1] However, research is currently being directed to selectively produce *p*-xylene from low valued *o*- and *m*-xylene. Regrettably, how much *p*-xylene is theoretically obtainable from *m*-xylene conversions is very much limited by thermodynamics. As a result, researchers and scientists are at work to attempt to overcome the thermodynamic limitations associated with transformation reactions of xylenes.

The introduction of ZSM-5 in xylene transformation process by Mobil workers in the early 1970s was clearly a milestone. Since the commercialization of the process, selective preparation of *p*-xylene from the isomerization of *o*- and *m*-xylene over ZSM-5 has been investigated in detail by quite a number of investigators [2-14]. The interest directed on ZSM-5 is a result of its high activity and shape selectivity. ZSM-5 zeolite presents very strong shape selectivity as a result of their geometry and architecture of their channel systems. Being a medium-pore size zeolite with a pore diameter of about 0.55nm, *reactant shape selectivity* (which restricts or promotes transportation of reactant molecule into the zeolite channels) and *restricted transition state shape selectivity* (which prevents the formation of bulky reaction intermediates) play very significant roles in its reactions [15-17]. As a result of its strong shape selectivity, ZSM-5 is a suitable catalyst for the synthesis of alkyl and dialkyl benzenes, particularly their *para*-isomers. [18]

Xylene transformation process on ZSM-5 zeolites is a complicated process. In addition to isomerization, dealkylation, disproportionation, and transalkylation reactions might also be present. The complexity of the transformation reactions and the interplay of diffusion and chemical reactions have often led to different reaction pathways.

Two reaction schemes have been used in the literature to model xylene transformation reactions. The first one is the triangle reaction path (Silvestri and Prater [2]; Robschlager and Christoffel [3]; Collins et al., [4]; Hsu et al., [5]; and Li et al.,[6]) where *o*-xylene could be converted directly into *p*-xylene and vice versa (*o*-xylene *p*-xylene). This is explained by the fast movement of the para isomer inside the porous catalyst which might cause an apparent 1,3 shift of the methyl group in the benzene ring [7]. The second scheme on the other hand, assumes that the reaction proceeds via 1,2-methyl shift only (*o*-xylene *m*-xylene *p*-xylene) where one of the methyl groups in *m*-xylene might shift to the adjacent positions through a series of consecutive, reversible 1,2-methyl shift mechanism and become *o*-xylene or *p*-xylene (Lanewola and Bolton [8]; Chutoransky and Dwyer [9]; Collins et. Al., [10]; Cortes and Corma [11,12]; Corma and Cortes [13]; and Do [14]).

Detailed kinetic studies on silica-alumina catalysts [11,13] have shown that xylene transformation reactions occur via the 1,2 shifts of the methyl group, with the conversion of *o*- to *p*-xylene (and vice versa) occurring only through *m*-xylene as an intermediate. Studies involving large pore zeolite catalysts (e.g., mordenite or Y-zeolite) have also concluded that mutual interconversion between *o*- and *p*- xylene is quite difficult, indicating that 1,2-methyl shift is the prevailing reaction path in the xylene transformation reactions [10,19,20]. Collins et al., [4] and Young et al., [7] have investigated xylene isomerization over ZSM-5 in both liquid and gas phases, respectively. They concluded that due to diffusion limitations in the transport of *o*- and *m*-xylene through the ZSM-5 channels, these isomers are forced to transform to smaller molecules which include *p*-xylene. Further explanation for this behaviour was given by Cappellazzo [21] in their study of kinetics of shape selective xylene isomerization over ZSM-5 catalyst. They pointed out that due to the much more pronounced diffusional limitations for *o*- and *m*-xylene than for *p*-xylene, a multistep interconversion occurs in the zeolite channels, in which the smaller *p*-xylene has a much higher probability of diffusing in the bulk phase while *o*- and *m*-xylene are retained for longer times resulting in further isomerization. The net results as they indicated is the apparent formation of *p*-xylene directly from *o*-xylene in agreement with the 1,3-methyl shift reaction scheme.

Li et al., [6] used a pulse microreactor-chromatograph technique to study the xylene isomerization reaction over HZSM-5 zeolite catalyst. Their reported activation energies indicated that the transformation of *m*-xylene to *o*- or *p*-xylene, *o*-xylene to *m*- or *p*-xylene, and *p*-xylene to toluene are controlled by reaction, and the conversion of *p*-xylene to *m*- or *o*-xylene is in the transition regime of diffusion and reaction in the zeolite channels. Hsu et al., [5] studied the simultaneous isomerization of ethyl-benzene and *m*-xylene on Pt-ZSM-5 zeolite catalyst in an integral reactor and proposed a kinetic model where all diffusional effects are lumped into the reaction rate constants. The reaction rate constants determined therefore included contributions from the resistances in the macro- and micropore diffusions and the axial diffusion in the catalyst bed.

Regarding the kinetics of xylene transformations over zeolitic catalysts, several modeling techniques have been applied to obtain the numerous kinetic parameters of this complex reaction system. Amongst the techniques employed in the literature include: analytical methods such as Wei-Prater method [4,9,10], Laplace transform [14], and finite integral transform [6,22]. Curve fitting method, such as Himmelblau method [5], and least-squares method [21,23] have also been applied. Recently, Iliyas and Al-Khattaf [24] in their investigation of xylene isomerization over Y-zeolite, obtained the various kinetic parameters of the overall xylene transformation reactions from simplified effective kinetic models applied to each xylene isomers. Similar modeling procedure will be used in the present investigation.

It is clear from the above literature that researchers are divided into two groups regarding xylene isomerization mechanism. One group believes in 1,3-methyl shift and the other does not. The present study is an attempt to resolve the controversy as to whether xylene isomerization reaction takes place consecutively (via 1,2 methyl shift) or through mutual interconversion of the three isomers (1,3 methyl shift). The kinetics of xylene transformation over ZSM-5 in a fluidized-bed reactor will be modeled using the "time on stream" decay model. The modeling procedure proposed in our previous work [24,25] will be employed to obtain the kinetic constants for the reaction. The result obtained in the present study will be compared to that reported earlier over USY zeolite [24].

2. Experimental Section

2.1 The riser simulator

All the experimental runs were carried out in the riser simulator. This reactor is novel bench scale equipment with internal recycle unit invented by de Lasa [26] to overcome the technical problems of the standard micro-activity test (MAT). For example, the low olefinity obtained from MAT reactor, due to its higher reaction time (> 75 s) as compared to the riser (< 15 s), non uniform coke deposition (150 mm long catalyst bed), and temperature/concentration gradient, which are eliminated by the well-mixed characteristics and intense fluidization of the riser simulator. The riser simulator is fast becoming a valuable experimental tool for reaction evaluation involving model compounds [27,28] and also for testing and developing new fluidized catalytic cracking in vacuum gas oil cracking [29,30].

The riser simulator consists of two outer shells, the lower section and the upper section, which allow one to load or to unload the catalyst easily, as illustrated in Fig. 1. The reactor was designed in such a way that an annular space is created between the outer portion of the basket and the inner part of the reactor shell. A metallic gasket seals the two chambers with an impeller located in the upper section. A packing gland assembly and a cooling jacket surrounding the shaft provide support for the impeller. Upon rotation of the shaft, gas is forced outward from the center of the impeller toward the walls. This creates a lower pressure in the center region of the impeller, thus inducing flow of gas upward through the catalyst chamber from the bottom of the reactor annular region where the pressure is slightly higher. The impeller provides a fluidized bed of catalyst particles as well as intense gas mixing inside the reactor. A detailed description of various riser simulator components, sequence of injection and sampling can be found in work by Kraemer [31].

2.2 Materials

The as-prepared ZSM-5 zeolite used in this work was spray-dried using kaolin as the filler and a silica sol as the binder. The resulting 60 μm catalyst particles had the following composition: 30 wt % zeolite, 50 wt % kaolin, and 20 wt % silica. The catalyst was calcined at 600^{o}C (873K) for 2 h. Analytical grade (99% purity) pure *m*-xylene, *p*- and

o-xylene were obtained from Sigma-Aldrich. All chemicals were used as received as no attempt was made to further purify the samples.

2.3 Catalyst characterization

The BET surface area was measured according to the standard procedure ASTM D-3663 using Sorptomatic 1800 Carlo Erba Strumentazione unit, Italy. The acid property of the catalyst was characterized by NH_3 temperature-programmed desorption (NH_3-TPD). In all the experiments, 50 mg of sample was out gassed at 400 ^oC (673 K) for 30 min. in flowing He and then cooled down to 100 ^oC (373 K). At that temperature, NH_3 was adsorbed on the sample by injecting pulses of 2 µl/pulse. The injection was repeated until the amount of NH_3 detected was the same for the last two injections. After the adsorption of NH_3 was saturated, the sample was flushed at 100 ^oC (373 K) for 1 h. with He to remove excess NH_3, and then the temperature was programmed at 10 ^oC (283 K) /min up to 850 ^oC (1123 K) in flowing helium at 30 ml/min. Flame ionization detector was used to monitor the desorbed NH_3.

2.4. Procedure

The experimental procedure in the riser simulator may be summarized as follows; a 80 mg portion of the catalyst was weighed and loaded into the riser simulator basket. The system was then sealed and tested for any pressure leaks by monitoring the pressure changes in the system. Furthermore, the reactor was heated to the desired reaction temperature. The vacuum box was also heated to around 250^oC (523 K) and evacuated at around 0.5 psi (3.45 kPa) to prevent any condensation of hydrocarbons inside the box. The heating of the riser simulator was conducted under continuous flow of inert gas (Ar), and it usually takes a few hours until thermal equilibrium is finally attained. Meanwhile, before the initial experimental run, the catalyst was activated for 15 min at 620^oC (893 K) in a stream of Ar. The temperature controller was set to the desired reaction temperature, and in the same manner, the timer was adjusted to the desired reaction time. At this point the GC is started and set to the desired conditions.

Once the reactor and the gas chromatograph have reached the desired operating conditions, the feedstock was injected directly into the reactor via a loaded syringe. After the reaction, the four-port valve immediately opens, ensuring that the reaction was terminated and the entire product stream sent online to the analytical equipment via a preheated vacuum box chamber.

2.5 Analysis

The riser simulator operates in conjunction with a series of sampling valves that allow, following a predetermined sequence, one to inject reactants and withdraw products in short periods of time. The products were analyzed in an Agilent 6890N gas chromatograph with a flame ionization detector and a capillary column INNOWAX, 60-m cross-linked methyl silicone with an internal diameter of 0.32 mm.

3. Kinetic Model Development

3.1 1,3 Methyl Shift

To develop a suitable kinetic model representing the overall transformation of xylenes, the reaction network shown in Scheme 1 is used for the 1,3 methyl shift. In this scheme, mutual interconversion of the isomers takes place. The reaction schemes 2-4, which are based on the transformation of each of the xylene isomers, will be employed to obtain the numerous kinetic parameters of Scheme 1.

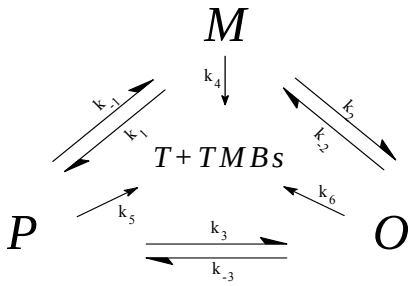

Scheme 1

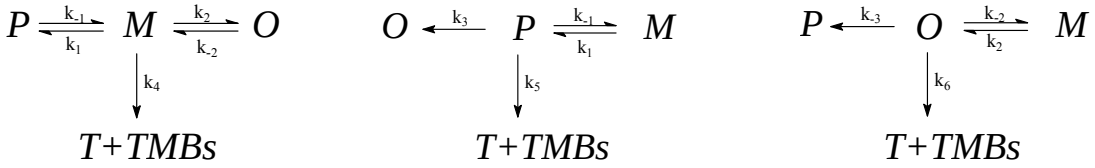

Scheme 2 Scheme 3 Scheme 4

The details of this analysis and the riser simulator mass balances based on the schemes 2-4 can be found in Ref. [24]. The concentration of any species *i* is related to its mass fraction as follows:

$$C_i = \frac{y_i W_{hc}}{MW_i V} \tag{1}$$

while the influence of temperature on the model parameters can be accounted for, through the following Arrhenius equation:

$$k_i = k_{0i} \exp\left(\frac{-E_i}{R}\left[\frac{1}{T} - \frac{1}{T_0}\right]\right) \tag{2}$$

T_o is the average reaction temperature introduced to reduce parameter interaction. As mentioned earlier, the time on stream" decay function ($\varphi = \exp[-\alpha t)]$) is employed in the mathematical models to account for catalyst deactivation.

In order to ensure thermodynamic consistency at equilibrium, the rate constants for *m*- to *p*-xylene, and *m*- to *o*-xylene reactions in the above equations are expressed as follows [23]:

$$k_{-1} = k_1/K_{pm} \tag{3}$$

$$k_{-2} = k_2/K_{om} \tag{4}$$

where $K_{pm} = (C_p/C_m)_{eq}$ and $K_{om} = (C_o/C_m)_{eq}$ are temperature-dependent equilibrium constants for both reactions, respectively. However, an average value can be computed for both constants since the thermodynamic equilibrium concentrations of the xylenes remain fairly constant within the temperature range of this work. The xylene equilibrium concentrations are obtained from a published work [32].

The overall kinetic model (based on scheme 1) can be obtained as follows:

$$\frac{dy_m}{dt} = -[(k_1 + k_2 + k_4)\, y_m - \frac{k_1}{K_{pm}} y_p - \frac{k_2}{K_{om}} y_o] \frac{W_c}{V} \exp[-\alpha t] \quad (5)$$

$$\frac{dy_p}{dt} = [k_1 y_m + \frac{k_3}{K_{pm}} y_o - (\frac{k_1}{K_{pm}} + k_3 + k_5) y_p] \frac{W_c}{V} \exp[-\alpha t] \quad (6)$$

$$\frac{dy_o}{dt} = [\, k_2 y_m + k_3 y_p - (\frac{k_2}{K_{om}} + \frac{k_3}{K_{om}} + k_6) y_o] \frac{W_c}{V} \exp[-\alpha t] \quad (7)$$

$$\frac{dy_d}{dt} = \left[\, k_4 y_m + k_5 y_p + k_6 y_o \,\right] \frac{W_c}{V} \exp[-\alpha t] \quad (8)$$

Each of the simplified kinetic models [ref. 24] consists of seven adjustable model parameters that have to be estimated before a solution is obtained. LSQCURVEFIT optimization routine in MATLAB has been employed to determine optimized parameters. The results obtained in this regard are presented and discussed in subsequent sections.

3.2 1,2 Methyl Shift

The reaction network to represent the overall transformation of xylenes via the 1,2 shift is shown in Scheme 5. In this scheme, one of the methyl groups in *m*-xylene might shift to the adjacent positions through a series of consecutive, reversible 1,2-methyl shift mechanism and become *o*-xylene or *p*-xylene. However, direct conversion of *p*-xylene to *o*-xylene is not possible. Simplified kinetic models as represented in reaction schemes 6-8 based on the transformation of each of the each xylene isomers, will be employed to obtain the numerous kinetic parameters of Scheme 5.

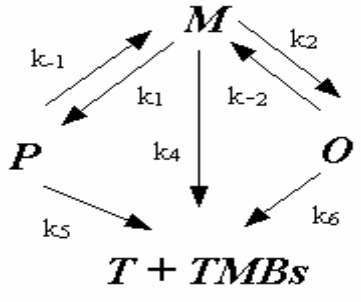

Scheme 5

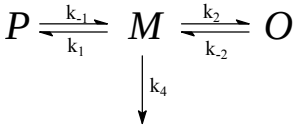

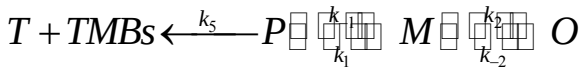

Scheme 6 Scheme 7

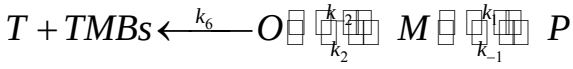

Scheme 8

It should be noted that the following assumptions were made in deriving the simplified models:

1. The isomerization and disproportionation reactions follow simple first-order kinetics.
2. An irreversible reaction path is assumed for disproportionation reaction. And the disproportionation reaction products toluene (T) and trimethylbenzenes (TMBs) are all as a result of the xylene reaction.
3. The reactor operates under isothermal conditions, justified by the negligible temperature change observed during the reactions.

The riser simulator mass balances based on the schemes 6-8 can be expressed as follows:

m-xylene (Scheme 6):

$$\frac{dy_m}{dt} = -[(k_1 + k_2 + k_4)\, y_m - \frac{k_1}{K_{pm}} y_p - \frac{k_2}{K_{om}} y_o]\frac{W_c}{V}\exp[-\alpha t] \qquad (9)$$

$$\frac{dy_p}{dt} = [k_1 y_m - \frac{k_1}{K_{pm}} y_p]\frac{W_c}{V}\exp[-\alpha t] \qquad (10)$$

$$\frac{dy_o}{dt} = [\, k_2 y_m - \frac{k_2}{K_{om}} y_o \,] \frac{W_c}{V} \exp[-\alpha t] \tag{11}$$

$$\frac{dy_d}{dt} = k_4 y_m \frac{W_c}{V} \exp[-\alpha t] \tag{12}$$

Note that the above equations (9-12) will be identical to Scheme 2 reactions.

p-xylene (Scheme 7):

$$\frac{dy_p}{dt} = -\left[\left(\frac{k_1}{K_{pm}} + k_5 \right) y_p - k_1 y_m \right] \frac{W_c}{V} \exp\left[-\alpha t\right] \tag{13}$$

$$\frac{dy_m}{dt} = \left[\left(\frac{k_1}{K_{pm}} y_p + \frac{k_2}{K_{om}} y_o \right) - \left(k_1 + k_2 \right) y_m \right] \frac{W_c}{V} \exp\left[-\alpha t\right] \tag{14}$$

$$\frac{dy_o}{dt} = \left(k_2 y_m - \frac{k_2}{K_{om}} y_o \right) \frac{W_c}{V} \exp\left[-\alpha t\right] \tag{15}$$

$$\frac{dy_d}{dt} = k_5 y_p \frac{W_c}{V} \exp\left[-\alpha t\right] \tag{16}$$

o-xylene (Scheme 8):

$$\frac{dy_o}{dt} = -\left[\left(\frac{k_2}{K_{om}} + k_6 \right) y_o - k_2 y_m \right] \frac{W_c}{V} \exp\left[-\alpha t\right] \tag{17}$$

$$\frac{dy_m}{dt} = \left[\left(\frac{k_2}{K_{om}} y_o + \frac{k_1}{K_{pm}} y_p \right) - \left(k_1 + k_2 \right) y_m \right] \frac{W_c}{V} \exp\left[-\alpha t\right] \tag{18}$$

$$\frac{dy_p}{dt} = \left(k_1 y_m + \frac{k_1}{K_{pm}} y_p \right) \frac{W_c}{V} \exp\left[-\alpha t\right] \tag{19}$$

$$\frac{dy_d}{dt} = k_6 y_o \frac{W_c}{V} \exp\left[-\alpha t\right] \tag{20}$$

Similarly, the "time on stream" decay function ($\varphi = \exp[-\alpha t)]$) is employed in the mathematical models to account for catalyst deactivation. Also, the rate constants for *m*- to *p*-xylene, and *m*- to *o*-xylene reactions are used to ensure thermodynamic consistency at

equilibrium.

The overall kinetic model (based on scheme 5) is thus as follows:

$$\frac{dy_m}{dt} = -\left[\left(k_1 + k_2 + k_4\right) y_m - \frac{k_1}{K_{pm}} y_p - \frac{k_2}{K_{om}} y_o\right] \frac{W_c}{V} \exp\left[-\alpha t\right] \tag{21}$$

$$\frac{dy_p}{dt} = \left[k_1 y_m - \left(\frac{k_1}{K_{pm}} + k_5\right) y_p\right] \frac{W_c}{V} \exp\left[-\alpha t\right] \tag{22}$$

$$\frac{dy_o}{dt} = \left[k_2 y_m - \left(\frac{k_2}{K_{om}} + k_6\right) y_o\right] \frac{W_c}{V} \exp\left[-\alpha t\right] \tag{23}$$

$$\frac{dy_d}{dt} = \left(k_4 y_m + k_5 y_p + k_6 y_o\right) \frac{W_c}{V} \exp\left[-\alpha t\right] \tag{24}$$

Similarly, each of the simplified models consists of seven adjustable model parameters that have to be estimated before a solution is obtained. Nonlinear regression analysis (LSQCURVEFIT) was used to fit the experimental data to the model and subsequently obtain the kinetic parameters.

4. Results and Discussion

4.1 Catalyst characterization

Zeolite catalysts for use in fluidized-bed reactors are often incorporated in amorphous matrix to achieve the desired fluidization of the catalyst particles. As a result, the determination of the crystallinity and phase purity of the zeolite samples in the presence of this matrix is important in catalytic reactions. The XRD patterns of the ZSM-5 catalysts obtained are in agreements with those reported in the literature, without the presence of extraneous peaks. The amount of desorbed NH_3 (total acidity) is 0.233 mmol/g. Pyridine adsorption was used to determine Lewis and Brønsted acidity using FTIR which shows 56% Brønsted and 44% Lewis sites. The measured BET surface area is 70 m^2/g. Furthermore, the ZSM-5 zeolite has a Si/Al ratio of about 50. However, the Na content in the zeolite was found to be negligible. Figure 2 shows the X-ray diffraction for the catalyst used.

4.2 Products distribution

The product distribution for the isomerization of *m*-xylene feedstock over the ZSM-5 zeolite catalyst is presented in Table 1. Tables 2 and 3 are the product distributions for the *p*- and *o*-xylene feeds, respectively. As shown in these tables, the major reaction products of each xylene reactants are: the other two xylene isomers, trimethylbenzenes and toluene. Traces of benzene and Tetramethylbenzenes were also observed, however, the yields of these products were very low. It can be seen from these tables that the yield of the various products increases with both reaction time and temperature. Since the yield of each isomer increases for all the isomerization reactions, it implies that with *p*-xylene as feed, both *m*- & *o*-xylene were found as primary products.

The conversion obtained with each xylene is compared in Fig. 3 at 450^{o}C (723 K). It can be observed from the figure and Tables 1-3, that *p*-xylene converts to other products more rapidly than the other two xylene isomers. This is indicative of the higher activity of *p*-xylene isomerization than both *m*- and *o*-xylene under the present experimental conditions with ZSM-5 zeolite catalyst. Furthermore, the conversion of *o*-xylene can be seen to be higher than *m*-xylene at all reaction temperatures and times studied. This is in

agreement with ref [33,34] where the diffusivity of *o*-xylene was found to be higher than that of *m*-xylene in ZSM-5. However, the latter results are in marked contrast to the results obtained with USY zeolite, reported by Iliyas and Al-Khattaf [24,25] under similar experimental conditions where the reactivity of the xylenes over USY zeolite was found to decrease in the following sequence: *p*-xylene > *m*-xylene > *o*-xylene.

4.3 Determination of Kinetic Parameters

The various kinetics parameters in eq 5-20 were determined from a nonlinear regression of the experimental data using MATLAB optimization routine (LSQCURVEFIT). The values of the pre-exponential factors and the apparent reaction constants and activation energies with their corresponding 95% confidence limits are presented in Table 4 (for 1, 3 shift) and Tables 5-7 (for 1,2 shift). The 95% confidence limits are used to judge the precision of the optimized parameters.

4.4 Discussion: Apparent Reaction Rate Constants and Activation Energies

4.4.1 1,3 shift

In the 1,3-methyl shift reaction mechanism, it is assumed that both 1,2 and 1,3 methyl shifts do occur. Based on this mechanism and using schemes 2 to 4, the values of the apparent kinetic parameters (*ko, E, &* α) were obtained and are reported in Table 4. k_1, k_2 *&* k_4 were obtained from Scheme 2 using *m*-xylene transformation data. While, k_{-1}, k_3 *and* k_5 were determined from Scheme 3 using *p*-xylene experimental data, and k_{-2}, k_{-3}, *&* k_6 were arrived at from *o*-xylene data using Scheme 4. The 95% confidence limits (CL) of each of the obtained parameters have been calculated and are shown in the table. Since the 95% CL are all very small as compared to the values of the parameters being determined, the obtained parameters are thus accurate and precise.

From the values of these parameters, it can be seen that the order of magnitude of the reaction rate constants for the unimolecular isomerization reaction is as follows: $k_{-1} > k_{-2} > k_1 > k_2 > k_{-3} \approx k_3$. The rate constant for the isomerization of *p*- to *m*-xylene (k_{-1}) is initially 3.6 greater that that of *p*- to *o*-xylene (k_3), and the ratio of (k_{-1}/k_3) decreases slightly with increasing reaction temperature. In our previous study on USY based catalyst [24], the rate constant for the isomerization of *p*- to *m*-xylene (k_{-1}) is initially about 1000

times greater than that of *p*- to *o*-xylene (k_3), and it decreased by half with an increase in the reaction temperature.

The rate constant for the isomerization of *o*- to *m*-xylene (k_{-2}) is twice that of *o*- to *p*-xylene (k_{-3}), and the ratio of (k_{-2}/k_{-3}) is almost constant with temperature as indicated in Table 4. In contrast to the USY-based catalyst [20], where the rate constant for the isomerization of *o*- to *m*-xylene (k_{-2}) was found to be 1400 times greater than that of *o*- to *p*-xylene (k_{-3}), and the ratio of (k_{-2}/k_{-3}) decreased to 500 with increasing temperature. The much lower values of the rate constants for *p*- to *o*-xylene (k_3) and *o*- to *p*-xylene (k_{-3}) in USY-based catalyst [24] is a clear indication that 1,3-methyl migration is difficult in USY-zeolite based catalysts as opposed to ZSM-5 where this difficulty is greatly reduced.

Furthermore, the rate constants for the isomerization of *m*- to *p*-xylene (k_1) and *m*- to *o*-xylene (k_2) are close to each other with the former being slightly higher. With respect to disproportionation reaction of xylenes, the rate constants obtained in this study (Table 4) show the following order of magnitude: $k_5 > k_4 \approx k_6$.

The higher rate constants for *p*-xylene reaction can be attributed to its very low adsorption strength as compared to *o*- and *m*-xylene [6]. Therefore, easier adsorption-desorption could result in faster methyl-shift during p-xylene conversion compared to the other two isomers. The near close rate constants for the *m*- to *p*-xylene (k_1) and *m*- to *o*-xylene (k_2) can be explained by the closeness of their estimated pre-exponential factors (0.259×10^{-3} and 0.215×10^{-3} m^3/kg of catalysts.s) and moreover, both involve migration of adjacent methyl group (1,2 shift).

The values of the apparent rate constants for *p*- to *o*-xylene and vice versa (k_3 & k_{-3}) are almost identical to the rate constants for the isomerization of *m*- to *o*-xylene (k_2). This clearly indicates that mutual interconversion between *p*- and *o*-xylene (a 1,3-methyl shift) occurs with the same rate as the conversion of *m*- to *o*-xylene (a 1,2-methyl shift). This is in marked contrast to the findings of ref. [24] based on estimated rate parameters over USY zeolite where 1,3-methyl migration was found to be difficult as compared to intramolecular 1,2-methyl shifts (i.e., *m*- to *p*-xylene, *m*- to *o*-xylene, and vice versa). It has even been suggested that xylene isomerization can only occur through *m*-xylene as an intermediate step and not directly as a single step for amorphous silica-alumina [11]. Our results show

that this is not the case for ZSM-5 zeolite catalyst under the present conditions. And our findings are in complete agreement with the results of Collins et al., [4] over ZSM-5.

This discrepancy between the two catalysts in our view might be due to the pore-size difference in the two zeolite catalysts. USY is a large pore zeolite which contains cages large enough to hold two or more aromatic molecules, larger than the pore size of ZSM-5. Aromatic molecules diffuse in and out of the super cage of USY zeolite without difficulty. But the diffusivity of xylene isomers varies greatly in ZSM-5; the diffusivity of *p*-xylene is about 10000 times that of *o*- or *m*-xylene [5]. As a result, *p*-xylene could diffuse quickly, while *o* or *m*-xylene might have to transform into molecules whose diameters are smaller before they can get out of the zeolite. This forced transformation includes xylenes transformation from *o*- or *m*-xylene to *p*-xylene leading to 1,3-methyl shift in agreement with Collins et al., [4]; Hsu et al., [5];Young et al., [7] and Cappellazzo et al.,[21].

It is observed from Table 4 as well, that the apparent rate constant for *p*- to *m*-xylene conversion (k_{-3}) is on the average 2.3 times the reverse reaction (k_3). Similarly, the apparent rate constant for *o*- to *m*-xylene conversion (k_{-2}) is on the average 2.0 times the reverse reaction (k_2). While for *p*- to *o*-xylene, the forward and the reverse apparent rate constants are almost identical with the reverse slightly higher. These findings are all consistent with the thermodynamic equilibrium amounts and with the findings of Collins et al. [4]. It is also remarkable to note that even though these kinetic parameters were obtained from three separate experimental data, the results are very consistent.

The results in Table 4 also show the apparent activation energies for various isomerization and disproportionation reactions. The values of our activation energies are generally lower than those reported by Hsu et al., [5], higher than those obtained by Akpolat and Gunduz [35], but in better agreement with those of Li et al., [6], over ZSM5 and Pt/ZSM5, respectively. It should be noted that the kinetic models, experimental conditions and the catalysts used in the above mentioned studies have considerable differences from ours. This may account for the deviations in the reported numerical values of the kinetic parameters.

The results in Table 4 also show that the apparent activation energy for the *m*- & *o*-xylene disproportionation reactions (E_4, E_6) are generally higher than those for

isomerization reactions. The apparent activation energy of *p*-xylene disproportionation reaction (E_5) has a much lower value as compared to both E_4 and E_6. This is in agreement with the fact the activation energy required to move out a methyl group as a result of xylene disproportionation should be higher than that required for intra-molecular methyl transfer by magnitudes of 3-4 kcal/mol [36]. The lower value of E_5 on the other hand, can be attributed to the formation of diphenyl- methane type transition intermediates during the disproportionation of *p*-xylene prior to further breakdown instead of the usual carbonium intermediates.

The activation energy for isomerization of *p*- to *m*-xylene (E_{-1}) is the lowest among all others, which indicate that the conversion of *p*-xylene to *m*-xylene is the easiest. The activation energy for *m*- to *o*-xylene isomerization (E_2=18.14 kJ/mole) is smaller than that *o*- to *m*-xylene isomerization (E_{-2}=21.23 kJ/mole), indicating that a lower energy barrier for *m*-xylene isomerization to *o*-xylene than the reverse reaction.

The apparent activation energies for the interconversion between *p*- and *o*-xylenes (E_3 *and* E_{-3}) are 17.31 and 19.47 kJ/mole, respectively. These values are very close to the activation energy value for *m*- to *o*-xylene isomerization reaction (E_2), 18.14 kJ/mole. This further confirms the possibility of interconversion between *p*- and *o*-xylenes.

Figures 4-6 show the comparison between the simplified model predictions and the experimental data at various temperatures. As observed in these plots, the model predictions compare favorably with the experimental data. This is also indicative that these models could also be used for kinetic data interpretation. Besides, the regression fit for the transformations of *m*-, *p*-, and *o*-xylenes gives a correlation coefficient of 0.99 for all.

To check the validity of the estimated kinetic parameters for use at conditions beyond those of the present study, the fitted parameters were substituted into the comprehensive model developed for this scheme, and the equations solved numerically using the fourth order Runge-Kutta method. The numerical results were compared with the experimental data as shown in Figure 7. It can be observed from this figure that the calculated results compare reasonably well with the experimental data, except at 623 K, where the product yields are slightly over predicted.

This provides significant evidence that the 1,3-methyl shift mechanism could be used for the interpretation of the data obtained during xylene transformation in the riser

simulator. Also, the good agreement between the model and experimental results proves that the "time on stream" decay model can be used to successfully model the overall xylene transformation.

4.4.2 1,2 Shift

In the 1,2-methyl shift reaction mechanism, it is assumed that only 1,2 methyl shift occurs. Based on this mechanism and using schemes 6 to 8, the values of the apparent kinetic parameters (*ko, E, & α*) were obtained and are reported in Tables 5, 6 & 7. k_1, k_2 & k_4 results are from Scheme 6 using *m*-xylene transformation data. While, k_{-1}, k_2 *and* k_5 values were obtained from Scheme 7 using *p*-xylene experimental data, and k_{-2}, k_1, & k_6 are obtained from *o*-xylene data using Scheme 8. The 95% confidence limits (CLs) of each of the obtained parameters have been calculated and are shown in the respective tables. The 95% CLs reported in Table 5 are satisfactory for all parameters; however, they are unacceptable for k_2 (Table 6) and k_{-2} (Table 7) as their values far exceed the determined apparent activation energies for k_2 and k_{-2}. Thus, k_2 and k_{-2} predictions and their respective activation energies are suspects, as their numerical values are statitistically meaningless as far as the 95% confidence limits are concerned. This suggests that 1,2-methyl shift only may not be an accurate representation of *p*- and *o*-xylene transformation mechanism over ZSM-5.

It is observed from Tables 5 and 7 as well, that the apparent rate constant for *o*- to *m*-xylene conversion (k_{-2}) is on the average 45 times the reverse reaction (k_2), inconsistent with the thermodynamic equilibrium compositions. Furthermore, the apparent rate constants at different temperatures for *m*- to *o*-xylene conversion (k_2) calculated from *m*-xylene data (Table 5) are different from those calculated from *p*-xylene transformation data (Table 6). Similarly, the apparent rate constants at different temperatures for *m*- to *p*-xylene conversion (k_1) calculated from *m*-xylene data (Table 5) are different from those calculated from *o*-xylene transformation data (Table 7). These all point to the inadequacy of the mechanism to properly represent the xylene reactions via the 1,2-methyl shift mechanism only.

In a recent study of xylene isomerization on modified HZSM-5 by Bauer et al. [37], they indicated that *m*-xylene rich feed isomerization to *o*- and *p*- xylene can be adequately

described by the monomolecular mechanism including 1,2-methyl group shift. However, the experimental data of isomerization of *o*-xylene feed under the same reaction condition was not matching the theoretical predictions based on consecutive reaction scheme (*o*-xylene *m*-xylene *p*-xylene), 1,2-methyl group shift. They were only able to overcome this anomaly by assuming direct conversion of *o*-xylene into *p*-xylene, 1,3-methyl group shift. This strongly supports with our findings, where apparent kinetic parameters (ko, E, & α) for (k_1, k_2 & k_4) obtained from Scheme 6 (identical to scheme 2) using *m*-xylene transformation data were found to be statistically sound regardless of the mechanism. But, isomerization results for *p*- and *o*-xylene feeds under identical reaction conditions showed mismatch between the experimental data and theoretical predictions if the 1,2-methyl shift mechanism was used.

Conclusions

The following conclusions can be drawn from transformations of the three xylene isomers over ZSM-5 in the riser simulator under the conditions of the present study:

1. The kinetics of vapor-phase isomerization of xylenes has been carried out over ZSM-5 zeolite catalyst using the riser simulator. A comprehensive kinetic model based on a triangular reaction network has been used to model the reactions. However, simplified effective kinetic models based on the isomerization of the pure xylene isomers are employed in obtaining the various kinetic parameters using the method of non linear regression analysis. A good comparison between experimental data and model predictions was obtained.

2. The reactivity of the xylene isomers was found to decrease in the sequence: *p*-xylene > *o*-xylene > *m*-xylene. This was attributed to the difference in the diffusion and adsorption capacities of the xylenes, which favors the isomers in the above sequence.

3. The results provide conclusive evidence that mutual interconversion between *p*- and *o*-xylene (a 1,3-methyl shift) occurs with the same rate as the conversion of *m*- to *o*-xylene (a 1,2-methyl shift) over ZSM-5 zeolite catalyst. Furthermore, kinetic parameters obtained using *m*-xylene transformation data were found to be statistically sound regardless of the mechanism. But, isomerization results for *p*- and *o*-xylene feeds under identical reaction conditions showed mismatch between the experimental data and theoretical predictions if the 1,2-methyl shift mechanism was used. The problem is resolved if 1,3-methyl shift mechanism is used instead. This therefore is evident that the 1,3 methyl shift reaction path better represents *p*- and *o*- xylene feed isomerization mechanism in ZSM-5 zeolite than the 1,2-methyl shifts only.

4. The contradicting difference in the earlier results of xylene transformation over USY based catalyst as compared to the results of the present study over ZSM-5 based catalyst is clearly as a result of the differences in the properties of these catalysts. USY has a larger pore size than that of ZSM-5. Thus, aromatic molecules can move in and out without hindrance. But in ZSM-5, only *p*-xylene is able to diffuse quickly, while *o* or *m*-xylene might have to transform into molecules whose diameters are smaller before they can get out of the zeolite. This forced transformation includes xylenes transformation from *o*- or *m*-xylene to *p*-xylene.

Acknowledgment

The authors gratefully acknowledge King Fahd University of Petroleum & Minerals for the financial support provided for this work under the project 255. We also wish to thank Mr. Mariano Gica for his useful collaboration on the experimental work.

Nomenclature

C_i concentration of specie *i* in the riser simulator (mole/m^3)

CFL confidence limit

E_i apparent activation energy of *i*th reaction, kJ/mol

k apparent kinetic rate constant (m^3/kgcat.s).

$$= k'_0 exp[\frac{-E_R}{R}(\frac{1}{T} - \frac{1}{T_0})$$

$k_o^{'}$ Pre-exponential factor in Arrhenius equation defined at an average temperature [m^3/kgcat.s], units based on first order reaction

MW_i molecular weight of specie *i*

r correlation coefficient

R universal gas constant, kJ/kmol K

t reaction time (s).

T reaction temperature, K

To average temperature of the experiment, 698 K

V volume of the riser (45 cm^3)

W_c mass of the catalysts (0.81 gcat)

W_{hc} total mass of hydrocarbons injected in the riser (0.162 g)

y_i mass fraction of *i*th component (wt%)

Greek letters

α apparent deactivation constant, s^{-1} (TOS Model)

φ apparent deactivation function, dimensionless

Literature Cited

1. The Innovation Group (TIG), *Chemical Market Reporter (CMR Online): Chemical Profiles – Paraxylene,* Schnell Publishing Company, 2004.

2. Silvestri, A. J., and Prater, C. D. J. *J. Phys. Chem* 68 (1964) 3268.

3. Robschlager, Christoffel, *Can. J. Chem. Eng.* 58 (1980) 517.

4. Collins, D. J., Medina, R. J., and Davis, B. H. *Can. J. Chem. Eng*. 61 (1983) 29.

5. Hsu, Y. S., Lee, T., and Hu, H. C. *Ind. Eng. Chem. Res.* 27 (1988) 942.

6. Li, Y., Chang, X. and Zeng, Z. *Ind. Eng. Chem. Res,* 31 (1992) 187.

7. Young, L. B., Butter, S. A., and Kaeding, W. W. *J. Catal.* 76 (1982) 418.

8. Lanewola, M. A., and Bolton, A. P. *J. Org. Chem*. 34 (1969) 3107.

9. Chutoransky, P., and Dwyer, F. G. *Advances in Chemistry Series* 121 (1973), 540.

10. Collins, D. J., Mulrooney, K. J., and Medina, R. J. *J. Catal.* 75 (1982) 291.

11. Cortes A., and Corma, A. *J. Catal.* 51 (1978) 338.

12. Cortes A., and Corma, A. *J. Catal*. 57 (1979) 444.

13. Corma A., and Cortes A. *Ind. Eng. Chem. Process Des. Dev.* 19 (1980) 263.

14. Do, D. *AIChE J.* 31, (1985) 574.

15. Weisz, P. B., and Frilette, V. J. *J. Phys. Chem*. 64 (1960) 342.

16. Csicsery, S. M. *J. Catal*. 19 (1970) 394.

17. Olson, D. H., and Haag, W. O. *ACS Symp. Ser.* 248 (1984) 275.

18. Cejka, J. and Wichterlova, B. *Cat. Rev.* 44 (2002) 375-421.

19. Hopper, J. R., Shigemura, D. S. *AIChE J*. 19 (1973) 1025.

20. Norman, G. H., Shigemura, D. S., and Hopper, J. R. *Ind. Eng. Chem. Prod. Res. Dev.,* 15 (1976) 41.

21. Cappellazzo, O., Messina, G. Cao. G., and Morbidelli, M. *Ind. Eng. Chem. Res.* 30 (1991) 2280.

22. Ma, Y. H., and Savage L.A., *AIChE J*. 33 (1987) 1233.

23. Gendy, T. S. *J. Chem. Technol. Biotechnol.,* 73 (1998) 109.

24. Iliyas, A., and Al-Khattaf, S. *Ind. Eng. Chem. Res.,* 43 (2004) 1349.

25. Iliyas, A., and Al-Khattaf, S. *Appl. Catal. A: Gen,* 269 (2004) 225.

26. de Lasa, H. T., US Patent 5 (102) (1992) 628.

27. Al-Khattaf, S, and de Lasa, H. I. *Ind. Eng. Chem. Res.* 40 (2001) 5398.

28. Al-Khattaf, S, and de Lasa, H. I. *Chem. Eng. Sc.*. 57 (2002) 4909.

29. Al-Khattaf, S, and de Lasa, H. I. *Appl. Catal. A: Gen,* 226 (2002) 139.

30. Al-Khattaf, S. *Appl. Catal. A: Gen,* 231 (2002) 293.

31. Kraemer, D. W., Ph.D. Dissertation, University of Western Ont., London, Canada 1991.

32. Stull, D. R., Westrum, E. F., Simke, G. C. *The Chemical Thermodynamics of Organic Compounds*, Wiley, New York, 1969, p.368.

33. Choudhary, V. R., Nayak, V. S., and Choudhary, T. V. *Ind. Eng. Chem. Res.* 36 (1997) 1812.

34. Mirth, G., Cejka, J., and Lercher, J. A. *J. Catal.* 139 (1993) 24.

35. Akpolat, O., and Gunduz, G. *J. Applied Sci.* 5 (2005) 236-248.

36. Cortes, A., and Sastre, E. *J. Catal.* 129 (1991) 177.

37. Bauer, F., Bilz, E., and Freyer, A. *Appl. Catal. A: Gen,* xxx (2005) xxx-xxx (in press)

List of Tables

Table 1: Product distribution (wt %) at various reaction conditions for *m*-xylene transformation

Temp (K)/ time (s)	Conv. (%)	Gas	Benzene	*m*-xylene	*p*-xylene	*o*-xylene	Toluene	*1,3,5* TMB	*1,2,4* TMB	*1,2,3* TMB	TeMB's
623											
3	3.55	-	-	96.45	1.15	0.91	0.47	0.14	0.32	0.04	0.12
7	4.26	-	-	95.74	1.50	1.32	0.63	0.19	0.42	0.05	0.14
10	7.03	-	-	92.97	2.55	1.95	1.15	0.35	0.79	0.09	0.14
15	9.41	-	-	90.59	3.91	2.46	1.40	0.42	0.99	0.11	0.12
673											
3	3.82	-	-	96.18	0.97	1.23	0.75	0.20	0.47	0.07	0.12
7	8.38	-	-	91.62	2.44	2.18	1.73	0.47	1.16	0.16	0.24
10	11.70	-	0.05	88.30	3.67	2.90	2.35	0.65	1.61	0.23	0.26
15	15.16	-	0.06	84.84	5.14	4.10	3.37	0.94	2.34	0.33	0.30
723											
3	4.50	-	-	95.50	1.18	1.38	0.91	0.24	0.57	0.09	0.13
7	10.14	-	0.07	89.86	2.70	2.48	2.28	0.60	1.51	0.23	0.28
10	13.94	-	0.08	86.06	3.87	3.27	3.14	0.83	2.11	0.32	0.33
15	18.91	0.05	0.15	80.09	5.28	4.40	4.68	1.21	3.15	0.48	0.42
773											
3	6.10	-	0.09	93.90	1.33	1.59	1.46	0.35	0.89	0.14	0.25
7	11.15	0.05	0.14	88.85	2.51	2.52	2.81	0.69	1.79	0.29	0.37
10	15.40	0.06	0.18	84.60	3.61	3.37	3.86	0.94	2.48	0.40	0.49
15	21.92	0.08	0.23	78.08	5.17	4.65	5.54	1.36	3.61	0.58	0.65

Table 2: Product distribution (wt %) at various reaction conditions for *p*-xylene transformation

Temp (K)/ time (s)	Conv. (%)	Gas	Benzene	*m*-xylene	*p*-xylene	*o*-xylene	Toluene	*1,3,5* TMB	*1,2,4* TMB	*1,2,3* TMB	TeMB's
623											
3	3.54	-	-	1.58	96.46	0.48	0.64	0.12	0.41	0.04	0.16
7	9.80	-	-	4.60	90.20	1.17	1.87	0.33	1.26	0.13	0.32
10	11.9	-	-	5.69	88.10	1.50	2.28	0.39	1.57	0.16	0.35
15	16.7	-	-	8.12	83.30	2.12	3.16	0.52	2.23	0.21	0.42
673											
3	5.65	-	-	2.63	94.35	0.75	1.00	0.20	0.66	0.08	0.23
7	12.10	-	0.05	5.36	87.90	1.60	2.36	0.52	1.53	0.20	0.36
10	16.31	-	0.06	7.30	83.69	2.03	3.28	0.66	2.16	0.26	0.48
15	22.88	-	0.08	10.41	77.12	3.32	4.75	1.05	3.15	0.41	0.60
723											
3	7.13	-	0.05	2.93	92.87	0.97	1.42	0.32	0.90	0.13	0.30
7	14.00	-	0.10	5.62	86.00	1.89	2.96	0.68	1.87	0.28	0.47
10	20.03	0.04	0.14	8.07	79.97	2.76	4.24	0.98	2.70	0.40	0.58
15	25.68	0.06	0.17	11.02	74.32	3.74	5.49	1.28	3.55	0.52	0.75
773											
3	7.61	-	0.08	2.93	92.39	2.06	1.62	0.36	0.99	0.16	0.32
7	16.01	0.08	0.21	5.63	83.99	2.23	3.73	0.82	2.24	0.36	0.58
10	19.92	0.09	0.23	7.29	80.08	2.82	4.51	1.01	2.76	0.44	0.64
15	27.30	0.12	0.28	10.27	72.70	3.93	6.03	1.37	3.74	0.59	0.77

Table 3: Product distribution (wt %) at various reaction conditions for *o*-xylene transformation

Temp (K)/ time (s)	Conv. (%)	Gas	Benzene	*m*-xylene	*p*-xylene	*o*-xylene	Toluene	*1,3,5* TMB	*1,2,4* TMB	*1,2,3* TMB	TeMB's
623											
3	2.25	-	-	1.02	0.50	97.75	0.20	0.04	0.18	-	0.11
7	4.42	-	-	2.04	1.03	95.58	0.49	0.07	0.43	0.06	0.12
10	6.27	-	-	2.60	1.62	93.73	0.64	0.09	0.56	0.08	0.12
15	8.25	-	-	4.04	2.26	91.75	0.77	0.11	0.69	0.10	0.11
673											
3	3.89	-	-	1.57	0.67	96.11	0.62	0.16	0.49	0.07	0.11
7	9.36	-	-	4.15	1.85	90.64	1.45	0.34	1.11	0.17	0.10
10	13.68	-	0.04	6.12	2.82	86.32	2.04	0.48	1.58	0.24	0.18
15	15.4	-	-	6.97	3.56	84.60	2.14	0.40	1.76	0.27	0.14
723											
3	5.50	-	0.04	2.01	0.86	94.50	1.09	0.27	0.77	0.12	0.14
7	12.60	0.05	0.08	4.74	2.10	87.43	2.49	0.61	1.77	0.28	0.26
10	16.65	0.05	0.09	6.73	3.00	83.35	3.03	0.74	2.22	0.35	0.26
15	22.41	0.07	0.10	9.29	4.24	77.59	3.93	0.95	2.90	0.46	0.30
773											
3	6.39	-	0.08	2.17	0.98	93.61	1.38	0.31	0.92	0.15	0.21
7	13.55	0.08	0.15	4.64	2.07	86.45	2.99	0.72	2.02	0.34	0.38
10	17.19	0.09	0.17	6.44	2.89	81.81	3.88	0.95	2.66	0.44	0.45
15	25.57	0.15	0.22	9.31	4.19	74.43	5.32	1.30	3.67	0.61	0.57

Table 4: Estimated kinetic parameters (1,3-methyl shift)

Temp, (K)	Rate constant $\boldsymbol{k_i}$ ($\times 10^4$), (m^3/kg of catalyst.s)								
	k_1	k_{-1}	k_2	k_{-2}	k_3	k_{-3}	k_4	k_5	k_6
623	2.00	4.84	1.47	2.71	1.33	1.33	2.08	3.74	1.65
673	2.39	5.48	1.91	3.68	1.71	1.76	3.13	4.85	2.81
723	2.78	6.11	2.39	4.78	2.11	2.24	4.44	6.06	4.44
773	3.18	6.71	2.91	6.01	2.55	2.76	6.03	7.37	6.62
$\boldsymbol{E_i}$ (kJ/mol)	12.37	8.75	18.14	21.23	17.31	19.47	28.44	18.07	37.07
95% CL	6.33	2.96	9.1	6.16	8.87	12.44	4.29	3.15	7.62
$\boldsymbol{k_{0i}}^{a}\times 10^3$ (m^3/kg of catalyst.s)	0.259	0.580	0.215	0.421	0.191	0.199	0.375	0.545	0.356
95% CL$\times 10^3$	0.04	0.04	0.03	0.05	0.03	0.04	0.04	0.04	0.06
$\alpha_{average}$ = 0.023 (95% CL of 0.015)									

[a]pre-exponential factor as obtained from equation (2)

Table 5: Estimated kinetic parameters (1,2-methyl shift) : *m*-Xylene transformation

Temp, (K)	Rate constant $\boldsymbol{k_i}$ ($\times 10^4$), (m^3/kg of catalyst.s)		
	k_1	k_2	k_4
623	2.00	1.47	2.08
673	2.39	1.91	3.13
723	2.78	2.39	4.44
773	3.18	2.91	6.03
$\boldsymbol{E_i}$ (kJ/mol)	12.37	18.14	28.44
95% CL	6.33	9.1	4.29
$\boldsymbol{k_{0i}}^{b}\times 10^3$ (m^3/kg of catalyst.s)	0.259	0.215	0.375
95% CL$\times 10^3$	0.04	0.03	0.04
α = 0.016 (95% CL of 0.015)			

[b]pre-exponential factor as obtained from equation (2)

Table 6: Estimated kinetic parameters (1,2-methyl shift) : *p*-Xylene transformation

Temp, (K)	Rate constant $\boldsymbol{k_i}$ ($\times 10^4$), (m^3/kg of catalyst.s)		
	k_{-1}	k_2	k_5
623	6.13	60.85	3.71
673	7.18	97.53	4.80
723	8.22	146.45	6.00
773	9.26	208.64	7.29
$\boldsymbol{E_i}$ (kJ/mol)	11.01	32.89	18.05
95% CL	2.68	37.74	3.26
$\boldsymbol{k_{0i}}^{c}\times 10^3$ (m^3/kg of catalyst.s)	0.770	12.04	0.539
95% CL$\times 10^3$	0.06	6.84	0.04
α = 0.024 (95% CL of 0.023)			

[c]pre-exponential factor as obtained from equation (2)

Table 7: Estimated kinetic parameters (1,2-methyl shift) : *o*-Xylene transformation

Temp, (K)	Rate constant $\boldsymbol{k_i}$ ($\times 10^4$), (m^3/kg of catalyst.s)		
	k_{-2}	k_1	k_6
623	66.59	3.75	1.68
673	76.84	5.11	2.82
723	86.93	6.66	4.39
773	96.79	8.40	6.48
$\boldsymbol{E_i}$ (kJ/mol)	9.98	21.48	36.03
95% CL	62.17	5.73	8.50
$\boldsymbol{k_{0i}}^{\mathbf{d}} \times 10^3$ (m^3/kg of catalyst.s)	8.191	0.586	0.355
95% CL$\times 10^3$	6.97	0.09	0.06
α = 0.024 (95% CL of 0.023)			

[d]pre-exponential factor as obtained from equation (2)

Figure Captions

Figure 1: (a) Schematic diagram of the Riser Simulator. (b) Schematic diagram of the Riser Simulator experimental set-up.

Figure 2: X-ray Diffraction for the catalyst used in the study

Figure 3: Comparison between the conversions of xylene reactants at different reaction times (723 K).

Figure 4: Comparison between experimental results and model predictions (—) based on *m*-xylene transformation (Scheme 2; 1,3-methyl shift): (A) *m*-xylene conversion, (B) *p*-xylene yields, (C) *o*-xylene yields, (D) T + TMBs yields. (♦) 623 K; (■) 673 K; (▲) 723 K; (×) 773 K.

Figure 5: Comparison between experimental results and model predictions (—) based on *p*-xylene transformation (Scheme 3; 1,3-methyl shift): (A) *p*-xylene conversion, (B) *m*-xylene yields, (C) *o*-xylene yields, (D) T + TMBs yields. (♦) 623 K; (■) 673 K; (▲) 723 K; (×) 773 K.

Figure 6: Comparison between experimental results and model predictions (—) based on *o*-xylene transformation (Scheme 4; 1,3-methyl shift): (A) *o*-xylene conversion, (B) *m*-xylene yields, (C) *p*-xylene yields, (D) T + TMBs yields. (♦) 623 K; (■) 673 K; (▲) 723 K; (×) 773 K.

Figure 7: Comparison between experimental results and numerical simulations (─) based on overall *m*-xylene transformation (Scheme 1; 1,3-methyl shift) (A) T = 623 K: (B) T = 673 K: (C) T = 723 K: (D) T = 773K. (○) *p*-xylene; (□)T+TMBs; (◊)*o*-xylene; (Δ) *m*-xylene.

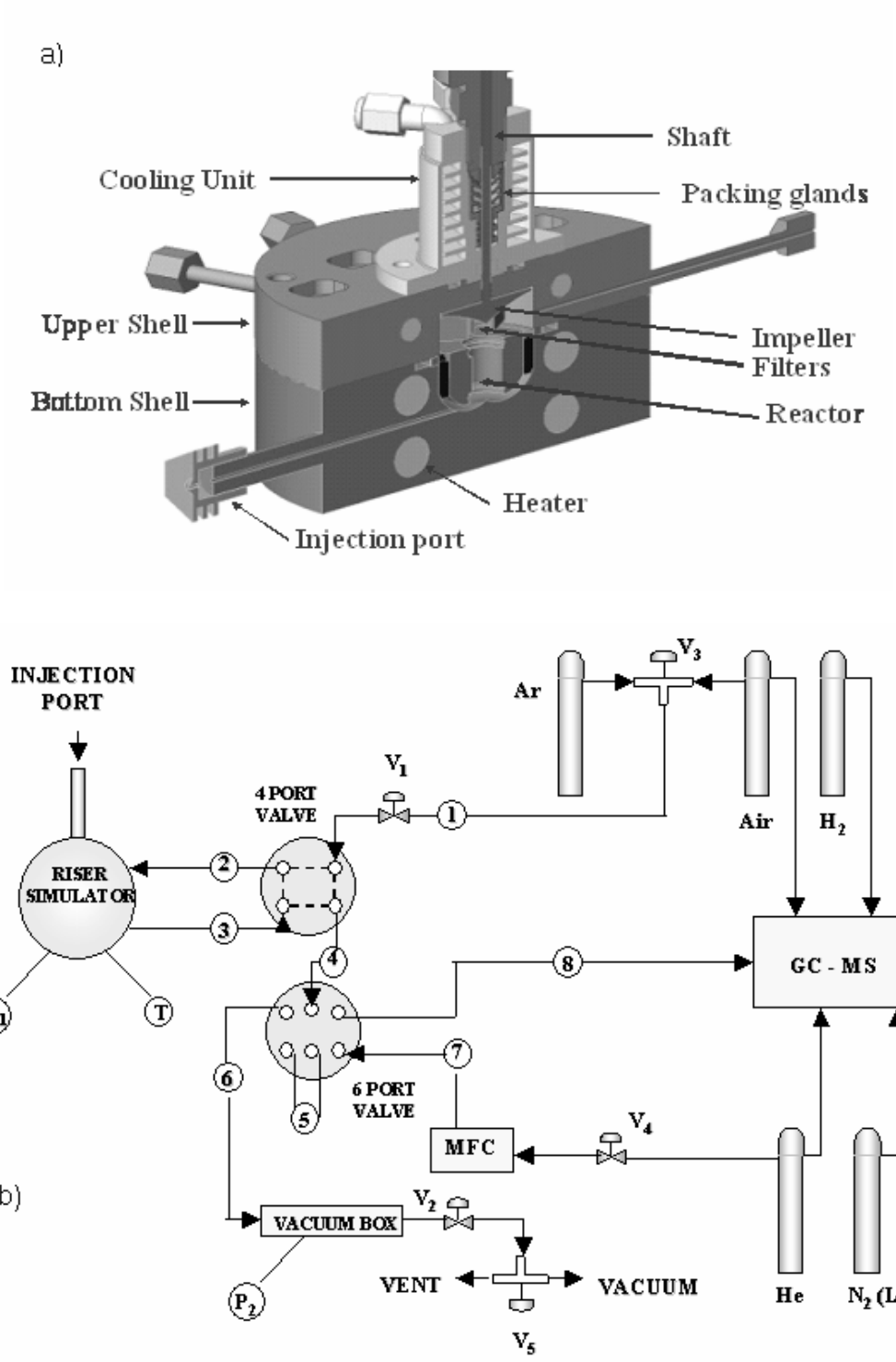

Figure 1: (a) Schematic diagram of the Riser Simulator. (b) Schematic diagram of the Riser Simulator experimental set-up.

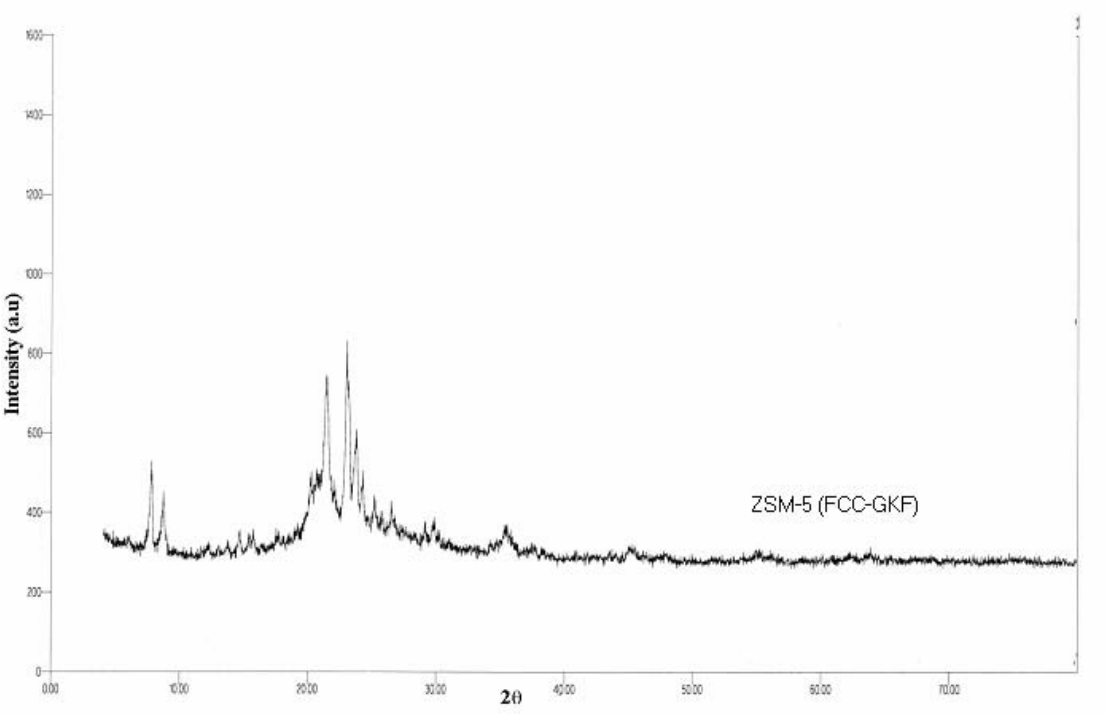

Figure 2: X-ray Diffraction for the catalyst used in the study

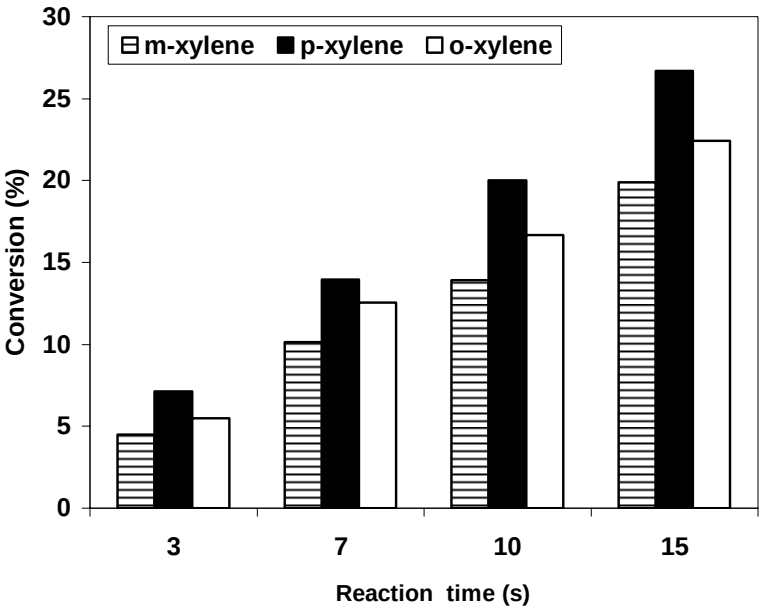

Figure 3: Comparison between the conversions of xylene reactants at different reaction times (723 K)

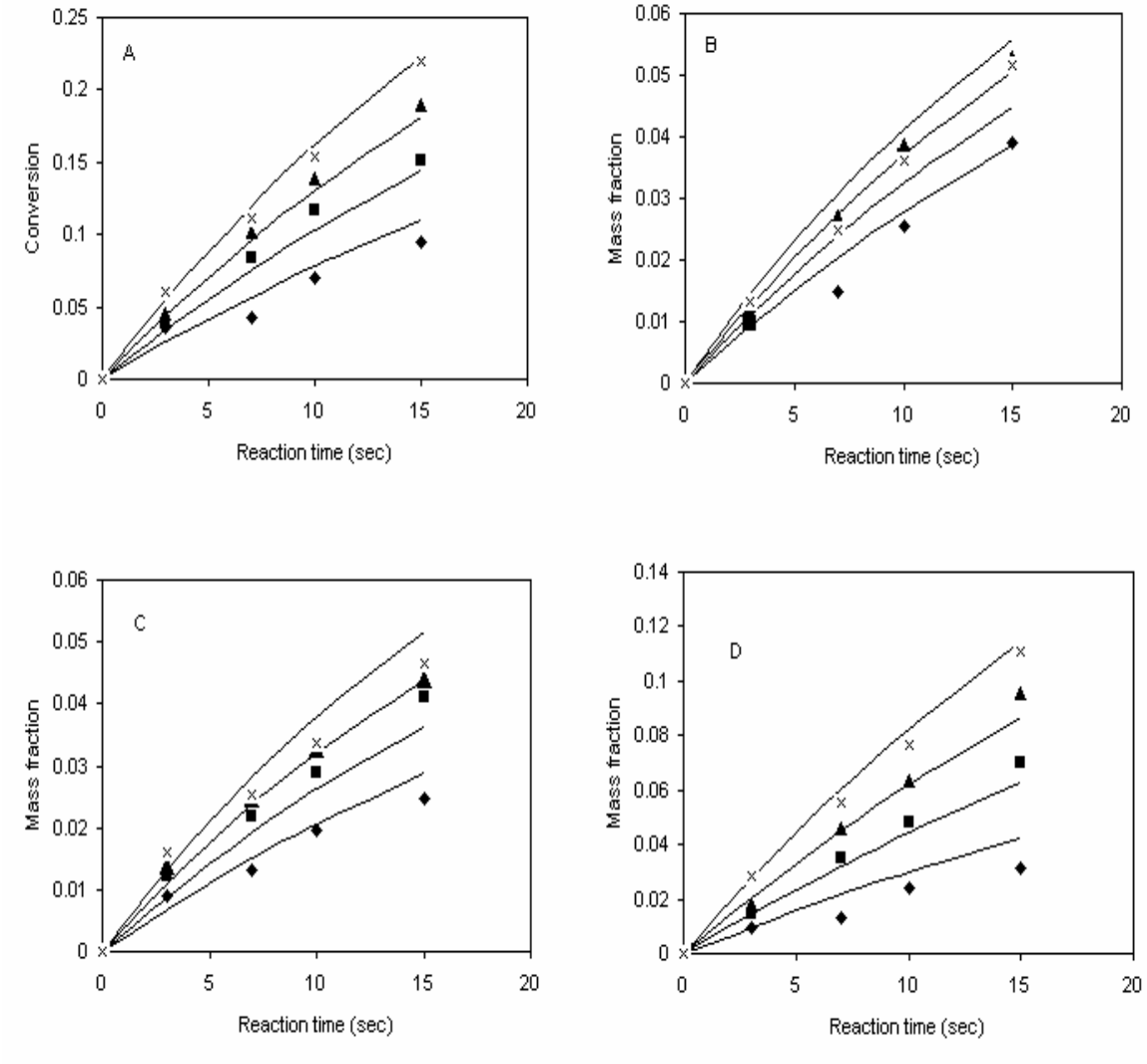

Figure 4: Comparison between experimental results and model predictions (—) based on *m*-xylene transformation (Scheme 2; 1,3-methyl shift): (A) *m*-xylene conversion, (B) *p*-xylene yields, (C) *o*-xylene yields, (D) T + TMBs yields. (♦) 623 K; (■) 673 K; (▲) 723 K; (×) 773 K.

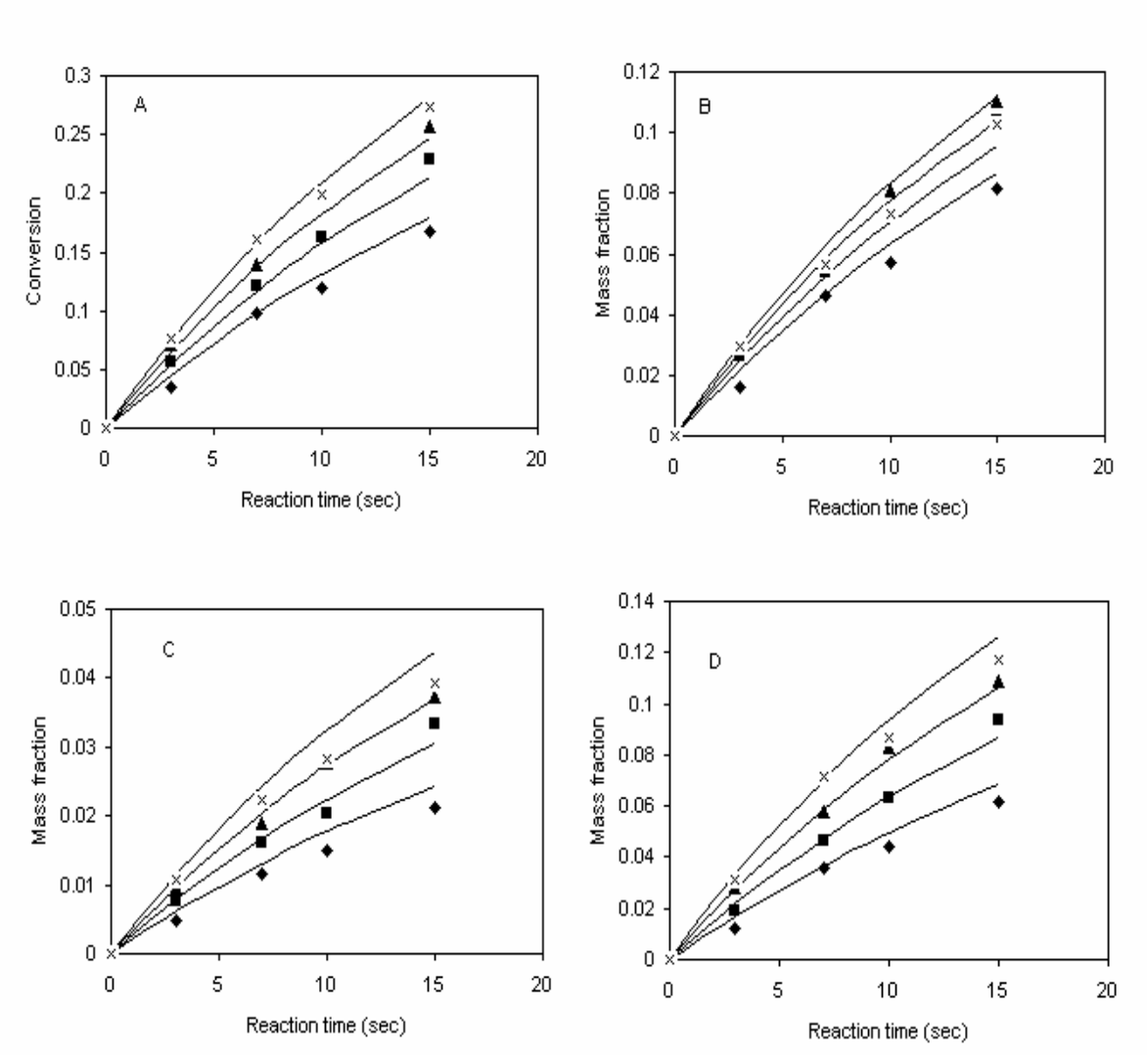

Figure 5: Comparison between experimental results and model predictions (—) based on *p*-xylene transformation (Scheme 3; 1,3-methyl shift): (A) *p*-xylene conversion, (B) *m*-xylene yields, (C) *o*-xylene yields, (D) T + TMBs yields. (♦) 623 K; (■) 673 K; (▲) 723 K; (×) 773 K.

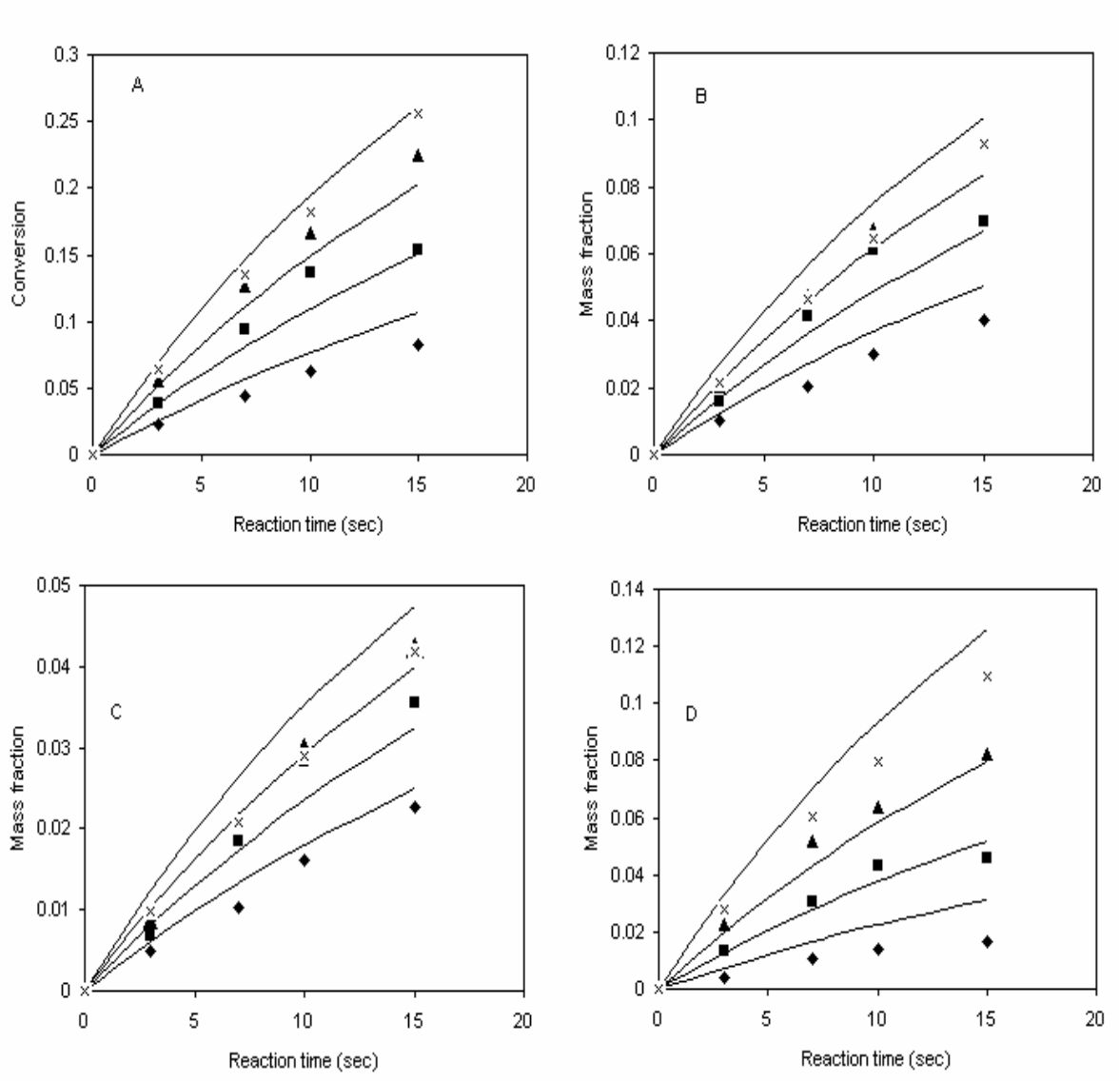

Figure 6: Comparison between experimental results and model predictions (—) based on *o*-xylene transformation (Scheme 4; 1,3-methyl shift): (A) *o*-xylene conversion, (B) *m*-xylene yields, (C) *p*-xylene yields, (D) T + TMBs yields. (♦) 623 K; (■) 673 K; (▲) 723 K; (×) 773 K.

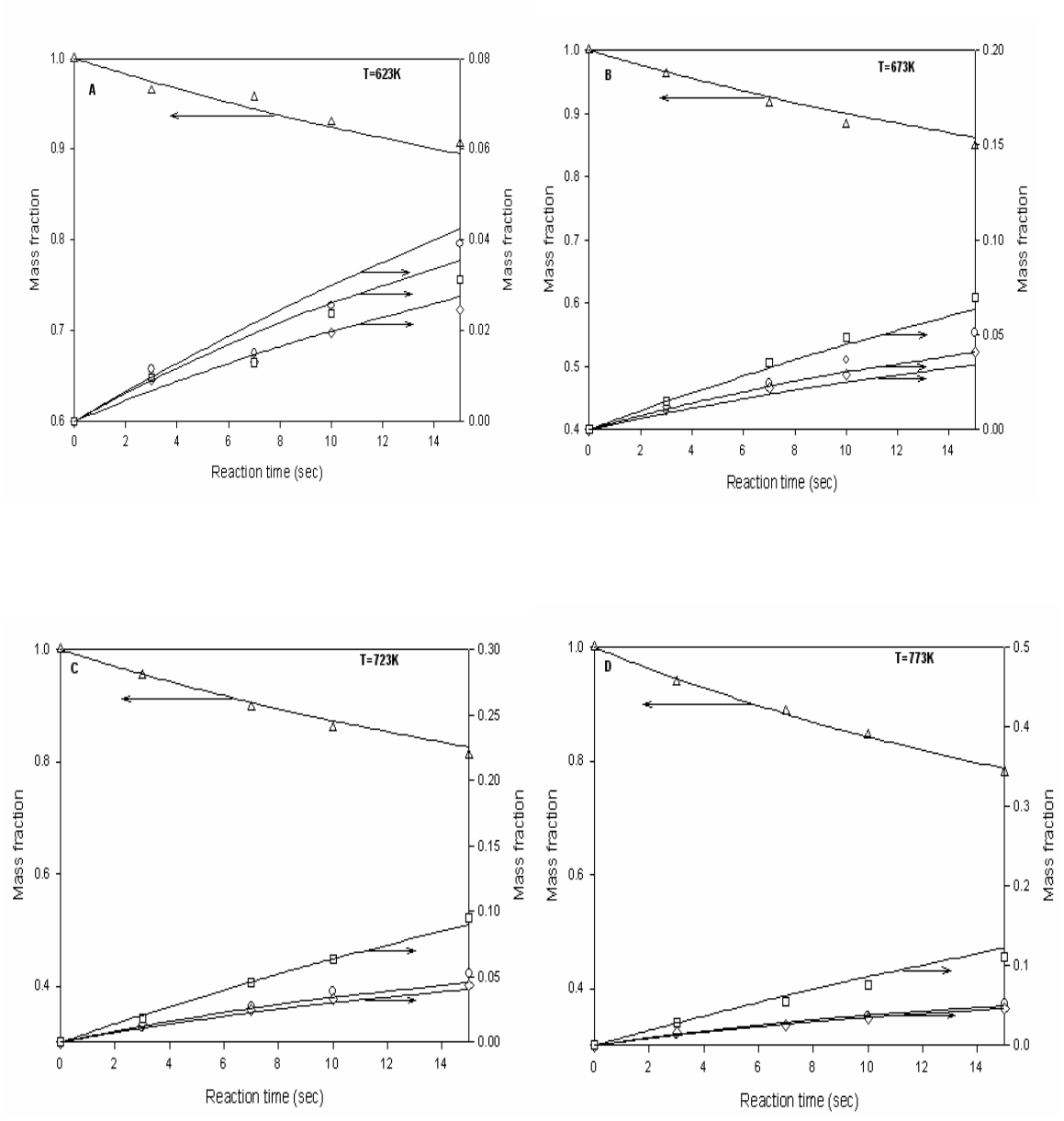

Figure 7: Comparison between experimental results and numerical simulations (─) based on overall *m*-xylene transformation (Scheme 1; 1,3-methyl shift) (A) *T* = 623 K: (B) *T* = 673 K: (C) *T* = 723 K: (D) *T* = 773K. (○) *p*-xylene; (□)T+TMBs; (◊)*o*-xylene; (Δ) *m*-xylene.